JOURNAL OF MATERIALS SCIENCE 30 (1995) 1653–1660

# Microstructural investigation of a rapidly solidified Ti–6Al–4V–1B–0.5Y alloy

Z. FAN
*Department of Materials, University of Oxford, Parks Road, Oxford OX1 3PH, UK*
A. P. MIODOWNIK
*Department of Materials Science and Engineering, University of Surrey, Guildford, Surrey, GU2 5XH, UK*
L. CHANDRASEKARAN, C. M. WARD-CLOSE
*Materials and Structures Department, Defence Research Agency, Farnborough, Hants GU14 6TD, UK*

A Ti–6Al–4V–1B–0.5Y (wt %) alloy has been prepared by consolidation of the melt-spun alloy fibres. The microstructures of the melt-spun fibre and the consolidated alloy were examined by different techniques. It was found that in the consolidated alloy, titanium boride and yttrium oxide particles have a refined particle size and a uniform distribution in the $\alpha(+\beta)$ matrix compared with the microstructure of the same alloy obtained by conventional ingot metallurgy. The boride phase in the consolidated alloy mainly has a needle-shaped morphology and has been identified by electron diffraction to be orthorhombic TiB with a B27 structure, while the yttrium oxide has a cuboidal morphology and has been identified as bcc $Y_2O_3$. Detailed TEM examination also revealed that yttrium addition has a strong influence on the TiB morphology by comparing the microstructures of Ti–6Al–4V–1B alloys with and without yttrium addition. Under similar processing conditions, the TiB phase in the consolidated alloys without yttrium addition mainly has a nearly equiaxed morphology with a finer particle size, while the TiB phase in the consolidated alloy with yttrium addition will mainly have a needle-shaped morphology. This effect of yttrium addition on the TiB morphology has been discussed in terms of heterogeneous nucleation and the reduced undercooling.

## 1. Introduction

In the past few years considerable efforts have been made to increase the elevated-temperature strength and creep behaviour of titanium-base alloys beyond those of conventional ingot metallurgy (IM) alloys by controlling the dispersion of hard second-phase particles [1]. However, in conventional IM temperature improvement has not been easy because of several difficulties, including (i) low solid solubility of dispersoid forming elements in titanium, (ii) heterogeneous distribution of dispersion, and (iii) rapid particle growth during the subsequent thermomechanical processing. On the other hand, rapid solidification (RS) techniques can potentially circumvent those problems. At high enough solidification rate the solid solubility of dispersoid-forming elements can be extended to a much higher level to produce a supersaturated solid solution. On annealing at suitable temperatures, the supersaturated solid solution can decompose to produce very fine stable dispersoids generally with a uniform distribution. Dispersoids which have been introduced to titanium alloy mixture are rare-earth (RE) elements or their oxides, sulphides, borides, carbides and silicides [2].

Boron has very low solid solubility in titanium with the equilibrium solid solubility in both $\alpha$- and $\beta$-titanium being less than 0.2 wt %[3]. Addition of boron to titanium alloys has, therefore, been limited in the conventional ingot metallurgy. Rapid solidification of liquid titanium alloys containing boron at a high cooling rate allows large departures from equilibrium constitution and results in large extension of the solid solubility of boron. It has been reported in the literature that this solubility can be extended beyond 10 at % [4, 5]. Thus RS processing can offer us an effective way of producing titanium solid solution with supersaturated boron. Upon subsequent consolidation of the RS product, titanium borides will precipitate within the titanium matrix to form a uniform distribution of fine boride reinforcement [2]. In addition to the formation of fine dispersoids, addition of yttrium to titanium can scavenge the interstitial oxygen which is detrimental to the mechanical properties such as ductility and fracture toughness [6]. It has been reported that RS can extend the equilibrium solid solubility of yttrium in titanium beyond 2 wt % [7].

0022–2461 

In the present research programme, the melt-spinning technique is being used to investigate the microstructural evolution of a rapidly solidified Ti–6Al–4V–1B–0.5Y alloy. The objectives of the present work were to establish the structural nature of the dispersoids (i.e. titanium boride and yttria) and to study the interaction between those two classes of dispersoids during rapid solidification and consolidation processings by comparing the microstructures of consolidated Ti–6Al–4V–1B alloys with and without yttrium addition.

## 2. Experimental procedure

The master Ti–6Al–4V alloy was supplied by the Defence Research Agency (UK), which contains 6.43 Al, 4.02 V, 0.19 Fe and 0.205 O (wt %, hereafter all alloy compositions are given in wt % unless otherwise stated). The Ti–6Al–4V–1B–0.5Y alloy was prepared by melting together the master alloy, $TiB_2$ powders (99.5% purity) and elemental yttrium (99.99% purity). $TiB_2$ and yttrium powders were wrapped in pure titanium thin foil before charging. Melting and melt-spinning were performed in a Marko's advanced melt spinner (Model 5T) in a stainless steel chamber with a high vacuum/inert gas atmosphere. The alloy was melted in a water-cooled copper hearth using a non-consumable tungsten electrode under a high-purity argon atmosphere. The chemically homogeneous melt was then delivered at a controlled rate to contact the circumferential surface of a rotating molybdenum wheel by which the melt is rapidly solidified as long fibres with a crescent-shaped cross-section, typically 100–300 μm wide and 40–100 μm thick. Some of the melt-spun fibres were found to be multi-layered ones. The melt-spun fibres were comminuted into finer particles with particle size less than 200 μm. The comminuted alloy powders were then filled into cylindrical titanium alloy cans which were baked in the temperature range 250–300 °C in vacuum ($10^{-5}$ torr; 1 torr = 133.322 Pa) before they were sealed by electron beam welding. This procedure was adopted to remove occluded gases in the powder compacts. The cans were consolidated by hot isostatic pressing (HIPing) at 900 °C, 300 MPa for 2 h, and then cooled to room temperature by furnace cooling. The HIPed alloy was subjected to a further 40% reduction in cross-section by hot pressing (forging) the can at 900 °C to produce a flat piece. A more detailed description of the experimental procedure and equipment used for preparation of the materials under investigation in this paper has already been given elsewhere [8].

Samples for optical microscopy (OM) and scanning electron microscopy (SEM) were polished by a standard metallographical technique. The polished specimens were chemically etched by using Kroll's reagent. Thin foils for transmission electron microscopy (TEM) were prepared in a "TENUPOL" unit using an electrolyte of 5 vol % perchloric acid in methanol. The polishing temperature was − 40 °C, the voltage 30 V, the current about 30 μA. TEM samples were also prepared by ion-beam thinning in a dual ion-beam miller at room temperature from both preelectrolytically polished discs and the mechanically polished discs. The voltage was set at 6 kV and the average specimen current was about 1 A. The thinning angle was 1.2 °. TEM observation was performed on a Jeol 200 CX STEM under an accelerating voltage of 200 kV.

## 3. Results

Microstructure of the alloy ingot solidified in the water-cooled copper hearth is presented in Fig. 1 as a backscattered scanning electron micrograph. The boride phase (black) has a needle-shaped morphology with an average length of about 20 μm, while the yttria phase (white) has a cuboidal morphology with the average particle size of 2 μm. The titanium matrix (grey) is fully martensitic. Fig. 1 also shows that, after solidification in the water-cooled copper hearth, the interfaces between the particles (titanium borides and yttria) and the matrix have been debonded. This is due to the large difference of coefficients of thermal expansion (CTE) between those particles and the titanium matrix.

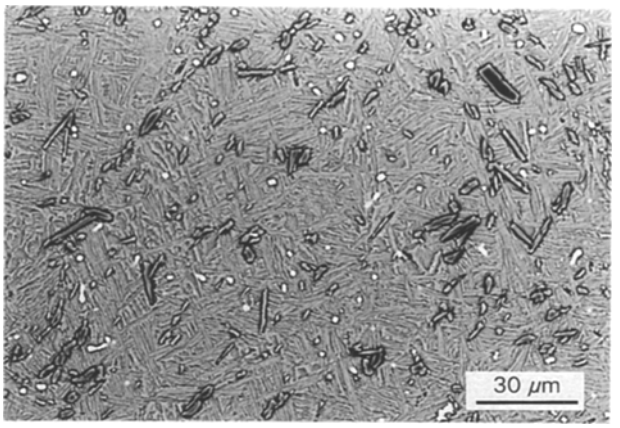


*Figure 1* SEM image (backscattered) showing the needle-shaped boride phase (black), cuboidal yttria particles (white) and the martensitic matrix (grey) in Ti–6Al–4V–1B–0.5Y ingot solidified in a water-cooled copper hearth.

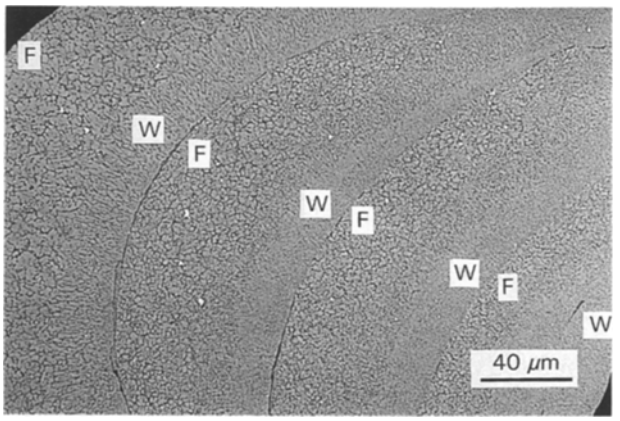


*Figure 2* SEM image (backscattered) showing the cross-section of a multi-layer melt-spun fibre. For a single layer, there are two microstructural zones: the equiaxed dendrite zone at free side (F) and the columnar grain zone at wheel side (W). The coarse yttria particles (white) can also be seen in this micrograph.

The cross-section of the melt-spun fibre has a two-zone microstructure: the columnar grain zone at the wheel side and the equiaxed dendrite zone at the free side, as shown in Fig. 2 by a backscattered SEM image of a multi-layered fibre. This two-zone microstructure is typical of the all melt-spun titanium alloys containing boron [9]. It is worth noting in Fig. 2 that some coarse yttria particles are present in the as-melt-spun fibres. Owing to their large size ( $> 1$ μm) and random location, it is possible that those yttria particles are already present in the melt before melt spinning. The microstructure of the longitudinal section of a coarse melt-spun fibre is shown in Fig. 3. It is interesting to note that both cuboidal yttria and needle-shaped titanium boride particles are already present in the coarse melt-spun fibres although their size has been reduced to a finer scale compared with Fig. 1. These results indicate that the undercooling achieved during the melt spinning is not enough to keep all the boron and yttrium atoms in solid solution.

The general microstructure of rapidly solidified Ti–6Al–4V–1B–0.5 Y alloy after consolidation is presented in Fig. 4. Both yttria and titanium boride particles have a refined particle size and have a uniform distribution throughout the $\alpha(+\beta)$ matrix. The detailed TEM examination of the consolidated material, Fig. 5, indicates that the boride phase has a needle-shaped morphology with an average length being less than 1 μm, while the yttria has a cubic morphology with an average particle size of 50 nm. In addition, it is also observed that the yttria particles frequently form clusters in the titanium matrix, as shown in Fig. 6.

In order to establish the nature of the yttrium oxide, the conventional selected-area diffraction technique has been proved to be unsuccessful owing to their small size. However, by using a focused electron probe on a single small particle situated at the thinned edge of the TEM sample, microdiffraction patterns have been obtained. Three such microdiffraction patterns from an yttria particle are presented in Fig. 7, which can be indexed as b c c $Y_2O_3$ with a lattice parameter of $a = 1.060$ nm. The majority of the boride particles has a needle-shaped morphology with a large aspect ratio. TEM observation indicates that such boride needles are just occasionally twinned or faulted. In addition, a small fraction of nearly equiaxed boride particles are also observed in the consolidated alloy, which are heavily twinned and/or faulted, as shown in Fig. 8. It is believed that the needle-shaped boride particles are formed from the liquid alloy during the solidification processing, while the nearly equiaxed

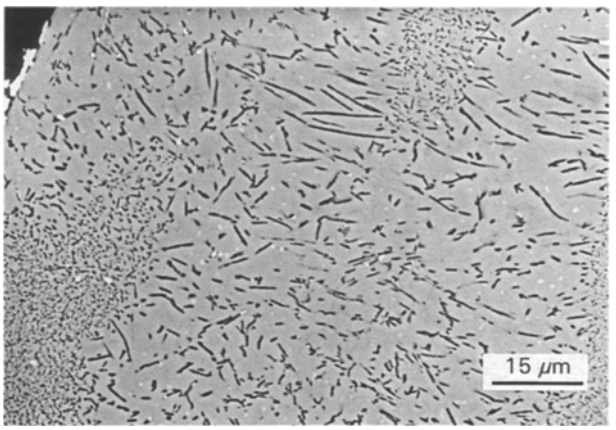


*Figure 3* SEM image (backscattered) showing the longitudinal section of a coarse melt-spun fibre. The needle-shaped boride phase (black) and cuboidal yttria particles (white) are already present in this melt-spun fibre.

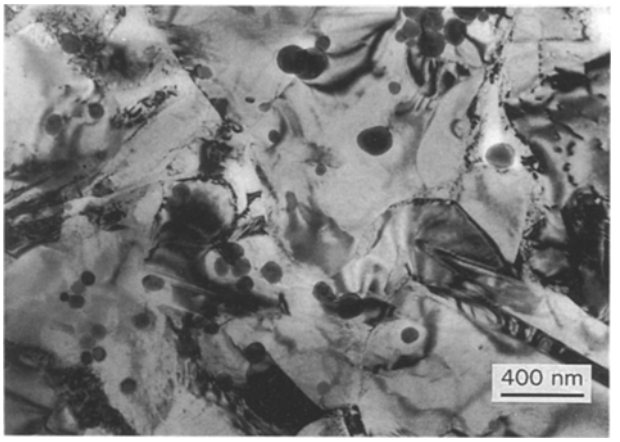


*Figure 5* Bright-field TEM image of the consolidated Ti–6Al–V–1B–0.5 Y alloy showing the detailed morphology of boride and yttria particles in the titanium matrix.

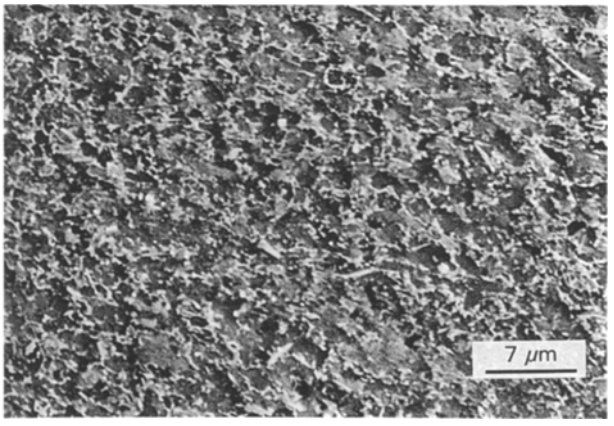


*Figure 4* SEM image (secondary) of the consolidated Ti–6Al–4V–1B–0.5 Y alloy showing the uniform distribution of fine boride and yttria particles in the titanium matrix.

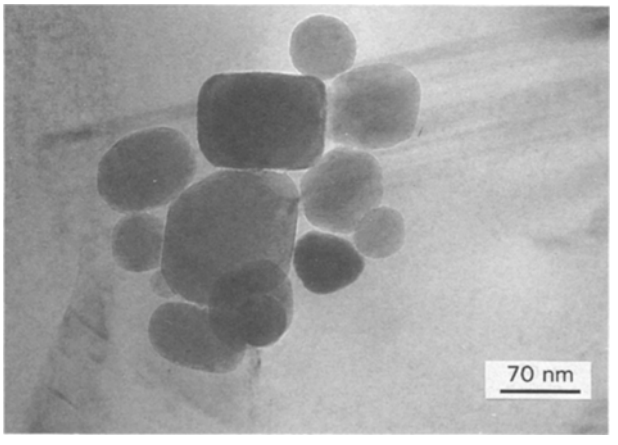


*Figure 6* Bright-field TEM image of the consolidated Ti–6Al–4V–1B–0.5 Y alloy showing a cluster of yttria particles in the titanium matrix.

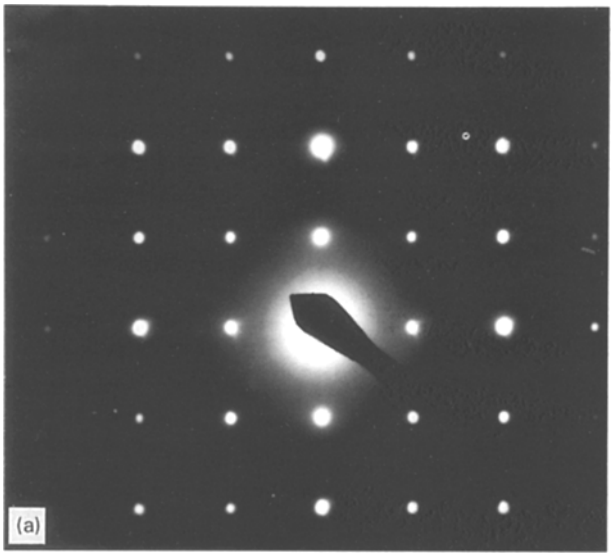


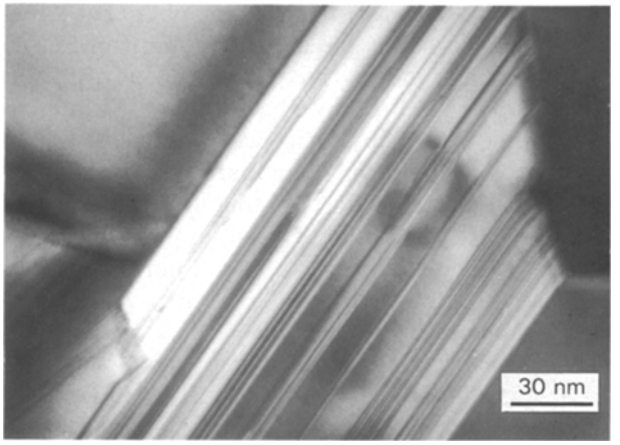


*Figure 8* Bright-field TEM image of a nearly equiaxed titanium boride particle in the consolidated Ti–6Al–4V–1B–0.5Y alloy showing the heavily twinned and/or faulted substructure.

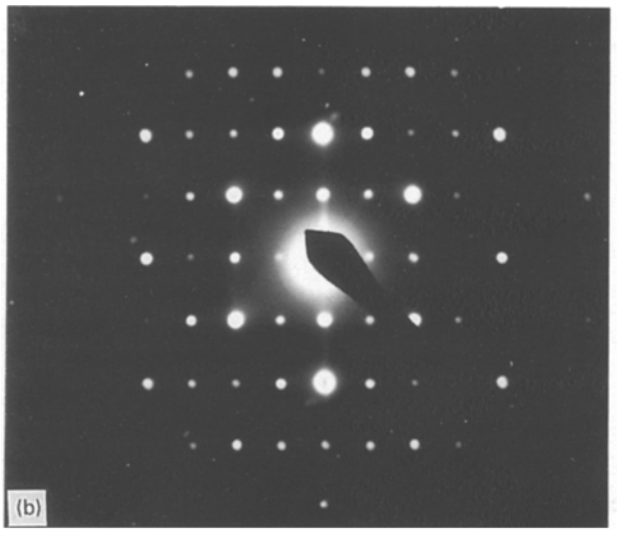



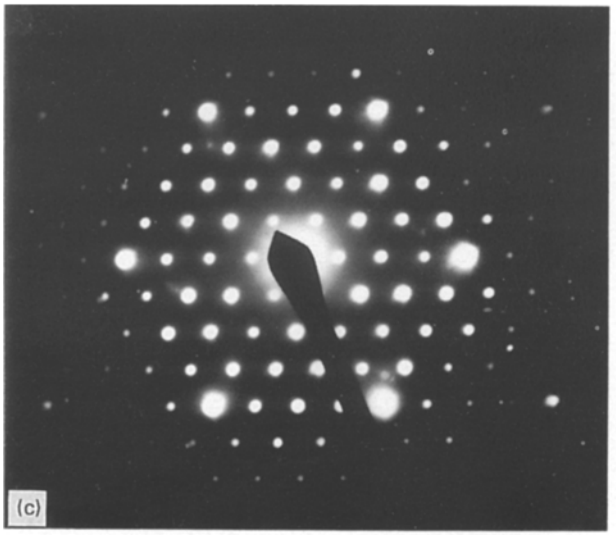


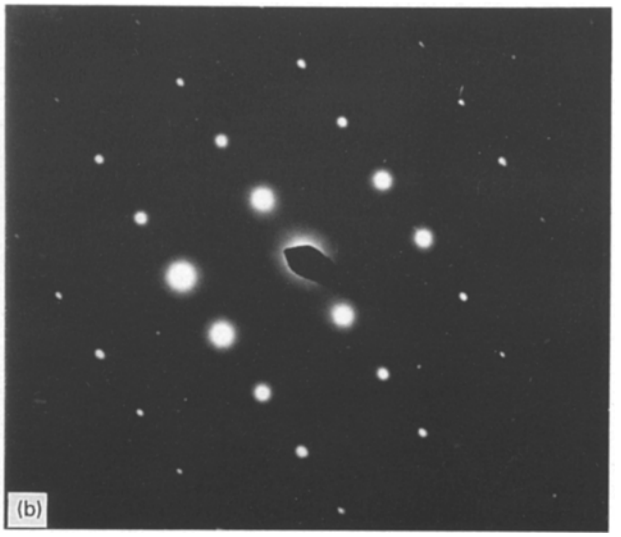


*Figure 7* Microdiffraction patterns obtained from an yttria particle situated at the thinned edge of the TEM sample. (a) $[0\,0\,1]_{Y_2O_3}$; (b) $[0\,1\,1]_{Y_2O_3}$; (c) $[\bar{1}\,1\,1]_{Y_2O_3}$.

*Figure 9* Selected-area diffraction patterns obtained from a needle-shaped titanium boride particle, which can be indexed as orthorhombic TiB. (a) $[\bar{1}\,0\,1]_{TiB}$; (b) $[1\,\bar{2}\,1]_{TiB}$; (c) $[\bar{1}\,1\,1]_{TiB}$.

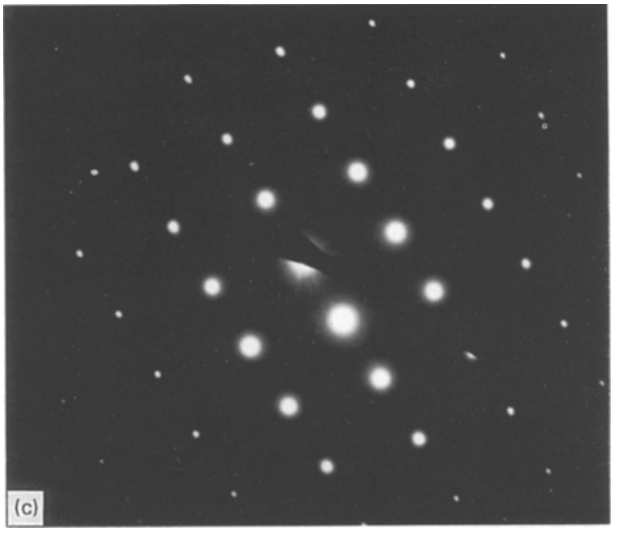


*Figure 9* (Continued).

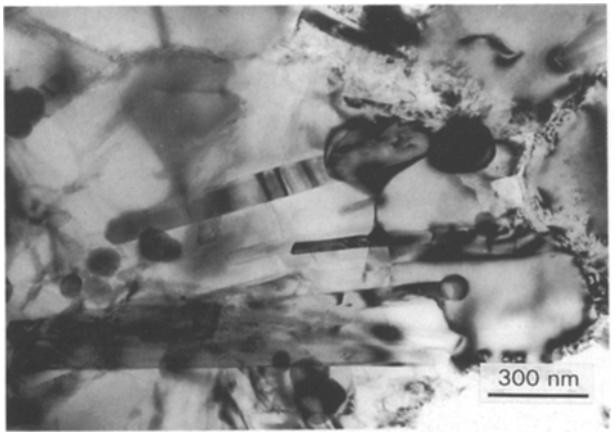


*Figure 10* Bright-field image of the consolidated Ti–6Al–4V–1B–0.5 Y alloy showing that TiB needles are often attached to yttria particles at one end.

ones with a heavily twinned and / or faulted substructure are formed through a solid-state reaction during the consolidation process [10]. Both the needle-shaped and the nearly equiaxed boride particles are identified by electron diffraction as TiB phase with a B27 structure, as evinced by three selected-area diffraction patterns in Fig. 9.

In addition, TEM examination of the consolidated alloy also revealed that there is a strong interaction between the cuboidal $Y_2O_3$ and needle-shaped TiB particles. The long TiB needles with their long axis being parallel to the $[0\,1\,0]_{TiB}$ direction are often attached at one end to $Y_2O_3$ particles. An example of such attachment is given in Fig. 10. This result may indicate that the long TiB needles are nucleated at the pre-existing solid $Y_2O_3$ particles during the solidification processing, rather than formed through a solid-state reaction.

Although the volume fraction of the β-phase in the consolidated alloy is just a few per cent, the β-grains are not single crystals. Fig. 11a shows the detailed morphology of a β-grain. Selected-area diffraction on such a β-grain indicates that after consolidation, the β-phase has decomposed into the equilibrium α-phase

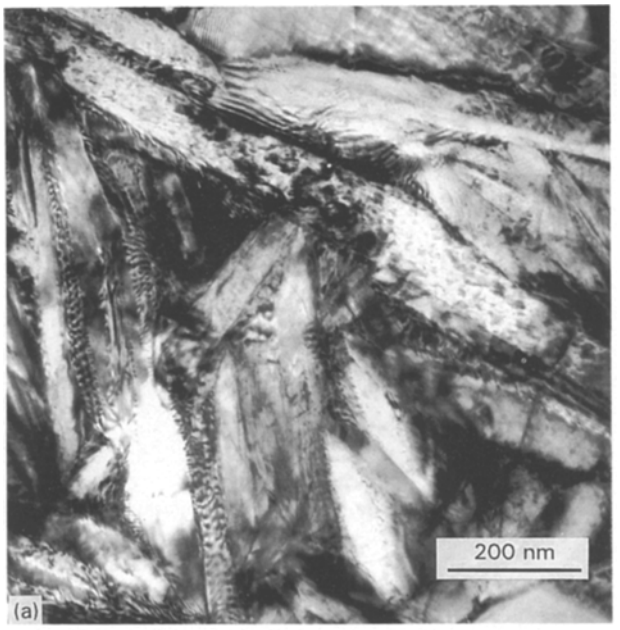


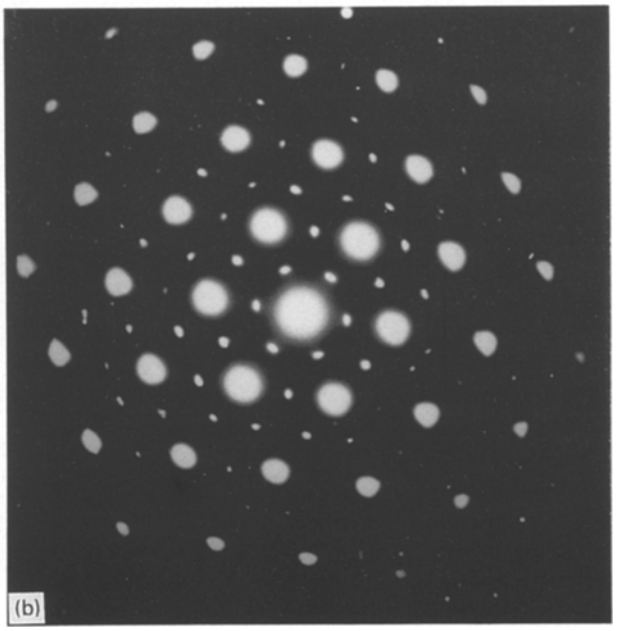


*Figure 11* (a) Bright-field TEM image of a β-grain in the consolidated Ti–6Al–4V–1B–0.5 Y alloy showing that the prior β-phase has decomposed into α-phase after consolidation, (b) $[1\,1\,1]_\beta$ zone axis pattern superimposed with three $\langle 1\,1\,\bar{2}\,0\rangle_\alpha$ patterns.

which obeys the Berger's orientation relationship. The obtained $[1\,1\,1]_\beta$ pattern is presented in Fig. 11b, where three $\langle 1\,1\,\bar{2}\,0\rangle_\alpha$ patterns are superimposed on the $[1\,1\,1]_\beta$ pattern.

## 4. Discussion

### 4.1. The effect of yttrium addition on the morphology of the TiB phase

Previous work by the same authors on rapidly solidified Ti–6Al–4V–XB alloys [10] showed that in melt-spun fibres of Ti–6Al–4V–1B alloy, no TiB precipitates were observed, although there was a boron concentrated region between the equiaxed

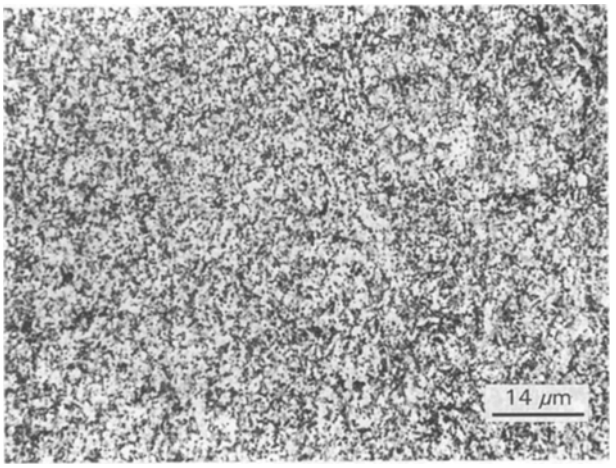


*Figure 12* Optical micrograph showing the uniform distribution of TiB particles in consolidated Ti–6Al–4V–1B alloy.


*Figure 13* Bright-field TEM image of the consolidated Ti–6Al–4V–1B alloy showing that the TiB phase mainly has a nearly equiaxed morphology with occasional presence of TiB needles.

dendrites and the columnar grains. In the consolidated Ti–6Al–4V–1B alloy, the majority of the TiB phase has a nearly equiaxed morphology and is distributed uniformly throughout the $\alpha(+\beta)$ matrix, as shown in Fig. 12, although a small population of needle-shaped TiB particles are also observed (see Fig. 13). A comparison between microstructures of Ti–6Al–4V–1B alloys with (Fig. 5) and without (Fig. 13) yttrium addition indicates that yttrium addition has a strong influence on the TiB morphology in consolidated alloys. The TiB phase in the consolidated alloy without yttrium addition mainly has a nearly equiaxed morphology with a finer particle size, while the TiB phase in the consolidated alloy with yttrium addition mainly has a needle-shaped morphology.

The above effect of yttrium addition on the TiB morphology can be understood from the following three aspects:

1. There are possibly solid $Y_2O_3$ particles in the melt before melt spinning (see Figs 2 and 3). The melting point of $Y_2O_3$ ($T_m = 2430\,°C$ [11]) is higher than that of TiB ($T_m = 2180\,°C$ [12]). In the present investigation, the melting of Ti–6Al–4V–1B–0.5Y alloy was conducted in a water-cooled copper hearth, where a large temperature gradient exists. In regions near the copper hearth, the temperature of the melt can be much lower than the melting point of $Y_2O_3$. Thus, solid $Y_2O_3$ particles can exist in the melt. In addition, according to Carlson [13] the Gibbs free energy of formation of $Y_2O_3$ is $\Delta G_f^0(Y_2O_3) = -1166.2\,kJ\,mol^{-1}$ at 2600 K, while from Murray's assessment [3], the Gibbs free energy of formation for TiB is $\Delta G_f^0(TiB) = -70.06\,kJ\,mol^{-1}$ at the same temperature, which is much larger than that for $Y_2O_3$. From the above thermodynamic data it can be concluded that solid $Y_2O_3$ particles are more likely to be present at low-temperature regions in the liquid alloy prior to the formation of TiB particles from the melt.

2. The solid $Y_2O_3$ particles in the melt can supply heterogeneous nucleation sites for subsequent formation of the TiB phase from the melt before the solidification of the matrix alloy. This argument is supported by the experimental evidence in Fig. 10, where the needle-shaped TiB particles are often attached to the cuboidal $Y_2O_3$ particles at one end. The other indirect evidence for this argument is that the TiB particles in the consolidated alloy are mainly needles with a large aspect ratio and rarely twinned or faulted, which are indicative that those TiB needles are formed from liquid phase during the solidification process rather than through a solid-state reaction [10].

3. The existence of solid $Y_2O_3$ particles in the melt can substantially reduce the undercooling which could be achieved during the melt spinning. The solid $Y_2O_3$ and TiB particles in the melt can act as heterogeneous nucleation sites for the prior β-grains during the subsequent solidification process and results in a lower undercooling. This reduced undercooling can, in turn, reduce the extended solid solubility of yttrium and boron and consequently decreases the volume fraction of the TiB particles formed through a solid-state reaction in the consolidated alloys. This explains why the majority of TiB particles in the consolidated alloy have a needle-shaped morphology with a large aspect ratio.

From the above discussion, it seems that addition of yttrium to rapidly solidified titanium alloys containing boron is not a good practice, as long as the mechanical properties are concerned. On the one hand, yttrium addition to titanium alloys containing boron can scavenge the detrimental oxygen in titanium solid solution and is likely to increase the ductility of the alloy [6]; on the other hand, yttrium addition leads to the formation of large TiB needles in the consolidated alloy, which will definitely decrease the ductility of the consolidated alloy.

## 4.2. The crystal structures of boride and yttrium oxide

The identification of the boride phase in RS titanium-base alloys containing boron has not been conclusive in the literature. For example, the TiB phase has been reported in RS Ti–6Al–3Sn–3Zr–0.25B

[14] and Ti–10Zr–6B (at %) alloys [15] without giving any detailed evidence; $TiB_2$ was also reported in RS Ti–15V–3Cr–3Sn–3Al–0.1–0.2B [16] and Ti–25V–2Er–0.02B alloy [17]. In the present investigation of rapidly solidified Ti–6Al–4V–1B–0.5Y alloy, the boride phase present in the consolidated alloy has been uniquely identified as TiB with an orthorhombic (B27) structure by electron diffraction (see Fig. 9). The lattice parameters of the TiB phase are in good agreement with the experimental results of Decker and Kasper [18] ($a = 0.612$ nm, $b = 0.306$ nm and $c = 0.456$ nm). One possible reason for this inconclusive identification is that other alloying elements may have a strong influence on the structure of boride. For instance, Hyman *et al.* [19] have suggested that increasing aluminium content may be favourable to $TiB_2$ formation.

According to the assessed Y–O binary phase diagram by Carlson [13], there are three types of $Y_2O_3$ which can exist in the nature: Type A is a high-temperature polymorph ($\beta$-$Y_2O_3$) and has a hexagonal structure with $P\bar{3}ml$ space group symmetry; Type B is a high-pressure polymorph ($\gamma$-$Y_2O_3$) and has a monoclinic structure with $C2/m$ space group symmetry; Type C is a low-temperature polymorph ($\alpha$-$Y_2O_3$) and has a cubic structure with $Ia\bar{3}$ space group symmetry. In previous work on rapidly solidified Ti–Al–Y alloys [7], the second-phase particles of size larger than 20 nm have been identified as $Y_2O_3$ with a bcc structure (Type C), while a fine distribution of precipitates in the size range of 8–20 nm was also observed, but the nature of this phase has not been established, although the precipitates were found to be rich in yttrium. In a RS Ti–5Sn–3Y alloy, Lu *et al.* [20] reported that the dispersoids were found to be rich in yttrium and tin and were identified by electron diffraction to be $Y_5Sn_3$. In the present study, all the yttrium oxide particles in rapidly solidified Ti–6Al–4V–1B–0.5 Y alloy have a particle size greater than 20 nm and have been identified by electron diffraction as $Y_2O_3$ with a bcc structure. Therefore, the identification of the nature of the yttrium-bearing particles in rapidly solidified titanium alloys has also not been conclusive. However, generally speaking, there will be a competition between oxygen and other alloying elements for formation of compounds with yttrium. Therefore, the nature of the eventual compound formed as a result of this connection will depend on the concentrations of yttrium, oxygen and other alloying elements and the thermodynamic conditions. Because of the large negative value for $\Delta G_f^0(Y_2O_3)$ quoted in Section 4.1, the oxygen content in the alloy may become the most important factor which dictates this competition. The yttrium-bearing particles are most likely to be $Y_2O_3$ in alloys with high oxygen content, as in the present case, while yttrium may form an intermetallic compound with other alloying elements in alloys with low oxygen content, for instance, $Y_5Sn_3$ in the case of Ti–5Sn–3Y alloy [20]. It is obvious that further experimental work is required to establish the structural nature of yttrium-bearing particles in rapidly solidified titanium alloys.

## 5. Conclusions

1. A Ti–6Al–4V–1B–0.5 Y (wt%) alloy has been prepared by consolidation of the rapidly solidified alloy fibres. Microstructural examination of the consolidated alloy revealed that the titanium boride and yttrium oxide particles have a refined particle size and a uniform distribution in the $\alpha( + \beta)$ matrix compared with the microstructure of the same alloy obtained by the conventional ingot metallurgy.

2. The boride phase in the consolidated alloy mainly has a needle-shaped morphology and has been identified by electron diffraction as TiB with a B27 structure, while the yttrium oxide has a cuboidal morphology and has been identified by microdiffraction to be bcc $Y_2O_3$.

3. Detailed TEM examination shows that yttrium addition has a strong influence on the TiB morphology by comparing the microstructures of Ti–6Al–4V–1B alloys with and without yttrium addition. Under similar processing conditions, the TiB phase in the alloy with yttrium addition mainly has a needle-shaped morphology with larger aspect ratio, while TiB particles in alloys without yttrium addition will mainly have a nearly equiaxed morphology. This effect of yttrium addition can be explained in terms of heterogeneous nucleation of TiB particles on the pre-existing solid $Y_2O_3$ particles and the reduced undercooling.

## Acknowledgement

The financial support by the Defence Research Agency, Farnborough, UK, is sincerely acknowledged.

## References

1. A. G. JACKSON, J. MOTEFF and H. F. FROES, in "Powder Metallurgy of Titanium Alloys", edited by F. H. Froes and J. E. Smugeresky (TMS-AIME, Warrendale, PA, 1980) p. 303.
2. C. SURYANARAYANA and F. H. FROES, *Int. Metall. Rev.* **36** (1991) 85.
3. J. L. MURRAY (ed.), "Phase Diagrams of Binary Titanium Alloys", (ASM International, Metals Park, OH, 1987) p. 33.
4. S. H. WHANG, *J. Mater. Sci.* **21** (1986) 2224.
5. S. H. WHANG and C. S. SHI, in "Rapidly Solidified Alloys and Their Mechanical and Magnetic Properties", Materials Research Society Symposia Vol. **58**, edited by B. C. Giessen, D. E. Polk and A. I. Taub (MRS, Boston, MA, 1986) p. 353.
6. B. B. RATH, B. A. MACDONALD, S. M. L. SASTRY, R. J. LEDERICH, J. E. O'NEAL and C. R. WHITSETT, in "Titanium '80: Science and Technology", Vol. 2, edited by. H. Kimura and O. Izumi, (The Metallurgical Society AIME, Warrendale, PA, 1980). p 1185.
7. D. G. KONITZER, B. C. MUDDLE and H. L. FRASER, *Metall. Trans.* **14A** (1983) 1979.
8. Z. FAN, A. P. MIODOWNIK, L. CHANDRASEKARAN and M. WARD-CLOSE, *J. Mater. Sci.* **29** (1994) 1127.
9. R. G. ROWE, T. F. BRODERICK, E. F. KOCH and F. H. FROES, in "Titanium-Rapid Solidification Technology", edited by F. H. Froes and D. Eylon, (The Metallurgical Society AIME, Warrendale, PA, 1986) p. 131.
10. Z. FAN, PhD thesis, University of Surrey, Guildford, UK (1993).
11. E. E. SHPIL'RAIN, D. N. KAGAN, L. S. BARKHATOV, L. I. ZHMAKIN and V. V. KOROLEVA, *High Temp. High Press.* **11** (1979) 539.

12. R. G. FENISH, *NRM* **138** (1964), PP.1-37.
13. O. N. CARLSON, *Bull. Alloy Phase Diagr.* **11** (1990) 61.
14. R. G. ROWE, E. F. KOCH, T. F. BRODERICK and F. H. FROES, in "Rapidly Solidified Materials", edited by P. W. Lee and R. S. Carbonara, (ASM, Metals Park OH, 1986) p. 107.
15. Y. Z. LU and B. C. GIESSEN, *Mater. Sci. Eng.* **98** (1988) 179.
16. T. KAINUMA and Y. KAWABE, in "Proceedings of the 6th World Conference on Titanium", Part II, edited by P. Lacombe, R. Tricot and G. Beranger (Les Editions de Physique, Les Ulis Cedex, France, 1989) p. 849.
17. Y. T. LEE, G. WIRTH, T. F. BRODERICK and F. H. FROES, *ibid.*, p. 837
18. B. F. DECKER and J. S. KASPER, *Acta Crystalogr.* **7** (1954) 77.
19. M. E. HYMAN, C. Mc CULLOUGH, J. J. VALLENCIA, C. G. LEVI and R. MEHRABIAN, *Metall. Trans.* **20A** (1989) 1847.
20. Y. Z. LU, B. C. GIESSEN and S. H. WHANG, in "Rapidly Solidified Alloys and Their Mechanical and Magnetic Properties", Materials Research Society Symposia, Vol. **58**, edited by B. C. Giessen, D. E. Polk and A. I. Taub (MRS, Boston, MA 1986) p. 377.

*Received 26 August*
*and accepted 4 October 1994*